The role of atmospheric aerosol concentration on deep convective precipitation: Cloud-resolving model simulations

Wei-Kuo Tao, Xiaowen Li, Alexander Khain, Toshihisa Matsui, Stephen Lang, and Joanne Simpson

Submitted to J. Geophy. Res.

Popular Summary

Aerosols and especially their effect on clouds are one of the key components of the climate system and the hydrological cycle [*Ramanathan et al.,* 2001]. Yet, the aerosol effect on clouds remains largely unknown and the processes involved not well understood. A recent report published by the National Academy of Science states "*The greatest uncertainty about the aerosol climate forcing - indeed, the largest of all the uncertainties about global climate forcing - is probably the indirect effect of aerosols on clouds NRC [2001].*" The aerosol effect on clouds is often categorized into the traditional "first indirect (i.e., Twomey)" effect on the cloud droplet sizes for a constant liquid water path and the "semi-direct" effect on cloud coverage. The aerosol effect on precipitation processes, also known as the second type of aerosol indirect effect, is even more complex, especially for mixed-phase convective clouds.

In this paper, a cloud-resolving model (CRM) with detailed spectral-bin microphysics was used to examine the effect of aerosols on three different deep convective cloud systems that developed in different geographic locations: South Florida, Oklahoma and the Central Pacific. In all three cases, rain reaches the ground earlier for the low CCN (clean) case. ***Rain suppression is also evident in all three cases with high CCN (dirty) case. However, this suppression only occurs during the first hour of the simulations. During the mature stages of the simulations, the effects of increasing aerosol concentration range from rain suppression in the Oklahoma case, to almost no effect in the Florida case, to rain enhancement in the Pacific case.*** These results show the complexity of aerosol interactions with convection.

The model results suggest that evaporative cooling is a key process in determining whether high CCN reduces or enhances precipitation. Stronger evaporative cooling can produce a stronger cold pool and thus stronger low-level convergence through interactions with the low-level wind shear. Consequently, precipitation processes can be more vigorous. For example, the evaporative cooling is more than two times stronger in the lower troposphere with high CCN for the Pacific case. Sensitivity tests also suggest that ice processes are crucial for suppressing precipitation in the Oklahoma case with high CCN.

The role of atmospheric aerosol concentration on deep convective precipitation: Cloud-resolving model simulations

Wei-Kuo Tao[1], Xiaowen Li[1,2], Alexander Khain[3], Toshihisa Matsui[1,2], Stephen Lang[4], and Joanne Simpson[1]

[1]*Laboratory for Atmospheres*
NASA Goddard Space Flight Center
Greenbelt, MD 20771
USA

[2]*Goddard Earth Sciences and Technology Center*
University of Maryland, Baltimore County
Baltimore, MD
USA

[3]*Department of Atmospheric Science*
Hebrew University of Jerusalem
Jerusalem, Israel

[4]*Science Systems and Applications, Inc.*
Lanham, Maryland

Submitted to JGR

April 2007

Corresponding author address: Dr. Wei-Kuo Tao, Code 613.1, Laboratory for Atmospheres, NASA GSFC, Greenbelt, MD 20771
email: tao@agnes.gsfc.nasa.gov

Abstract

A two-dimensional cloud-resolving model (CRM) with detailed spectral-bin microphysics is used to examine the effect of aerosols on three different deep convective cloud systems that developed in different geographic locations: South Florida, Oklahoma and the Central Pacific. A pair of model simulations, one with an idealized low CCN (clean) and one with an idealized high CCN (dirty environment), is conducted for each case.

In all three cases, rain reaches the ground earlier for the low CCN case. Rain suppression is also evident in all three cases with high CCN. However, this suppression only occurs during the first hour of the simulations. During the mature stages of the simulations, the effects of increasing aerosol concentration range from rain suppression in the Oklahoma case, to almost no effect in the Florida case, to rain enhancement in the Pacific case. The model results suggest that evaporative cooling is a key process in determining whether high CCN reduces or enhances precipitation. Stronger evaporative cooling can produce a stronger cold pool and thus stronger low-level convergence through interactions with the low-level wind shear. Consequently, precipitation processes can be more vigorous. For example, the evaporative cooling is more than two times stronger in the lower troposphere with high CCN for the Pacific case. Sensitivity tests also suggest that ice processes are crucial for suppressing precipitation in the Oklahoma case with high CCN. A brief comparison and review of other modeling studies are also presented.

1. Introduction

Aerosols and especially their effect on clouds are one of the key components of the climate system and the hydrological cycle [*Ramanathan et al.,* 2001]. Yet, the aerosol effect on clouds remains largely unknown and the processes involved not well understood. A recent report published by the National Academy of Science states "*The greatest uncertainty about the aerosol climate forcing - indeed, the largest of all the uncertainties about global climate forcing - is probably the indirect effect of aerosols on clouds NRC [2001].*" The aerosol effect on clouds is often categorized into the traditional "first indirect (i.e., Twomey)" effect on the cloud droplet sizes for a constant liquid water path [*Twomey,* 1977] and the "semi-direct" effect on cloud coverage [e.g., *Ackerman et al.,* 2000].

The aerosol effect on precipitation processes, also known as the second type of aerosol indirect effect [*Albrecht,* 1989], is even more complex, especially for mixed-phase convective clouds. A combination of cloud-top temperature and effective droplet sizes, estimated from the Advanced Very High Resolution Radiometer (AVHRR), has been used to infer the suppression of coalescence and precipitation processes for smoke [*Rosenfeld and Lensky,* 1998] and desert dust [*Rosenfeld et al.,* 2001]. Multi-sensor (passive/active microwave and visible and infrared sensors) satellite observations from the Tropical Rainfall Measuring Mission (TRMM) have been used to infer the presence of non-precipitating super-cooled liquid water near the cloud top due to over seeding from both smoke over Indonesia [*Rosenfeld,* 1999] and urban pollution over Australia [*Rosenfeld,* 2000]. In addition, aircraft

measurements have provided evidence of sustained supercooled liquid water down to -37.5°C in continental mixed-phase convective clouds [*Rosenfeld and Woodley,* 2000]. These findings further suggest that continental aerosols reduce the mean size of cloud droplets, suppressing coalescence and warm-rain processes, permitting more freezing of cloud droplets and associated latent heat release above the 0°C isotherm, and enhancing the growth of large hail and cold-rain processes [*Rosenfeld and Woodley,* 2000]. *Andreae et al.* [2004] analyzed *in-situ* observation during LBA-SMOCC (the Large-Scale Biosphere-Atmosphere Experiment in Amazonia-Smoke, Aerosols, Clouds, Rainfall, and Climate) campaign and found that increases in smoke and surface heat due to biomass burning tend to lead to higher cloud-top heights and the enhancement of cold-rain processes over the Amazon basin. *Linn et al.* [2006] examined multi-platform satellite data over the Amazon basin and found that high biomass burning-derived aerosols are correlated with the high cloud-top heights, large anvils, and more rainfall. *Koren et al.* [2005] examined cloud properties derived from the Moderate Resolution Imaging Spectroradiometer (MODIS) and found strong evidence that aerosols from pollution, desert dust and biomass burning systematically invigorate convective clouds over the Atlantic Ocean. Using long-term integrated TRMM-derived precipitation data, *Bell et al.* [2007] found a significant mid-week increase in summer-time afternoon thunderstorms over the southeast U.S., which coincides with a mid-week increase in ground-measured aerosol concentration. These findings are consistent with the notion that aerosols have a major impact on the dynamics, microphysics, and electrification properties of continental mixed-phase convective clouds [*Rosenfeld and Woodley,* 2000; *Orville et al.,* 2001; *Williams et al.,* 2002].

Table 1 summarizes the key observational studies identifying the microphysical properties, cloud characteristics, thermodynamics and dynamics associated with cloud systems from high-aerosol continental environments. For example, atmospheric aerosol concentrations can influence cloud droplet size distributions, warm-rain process, cold-rain process, cloud-top height, the depth of the mixed phase region, and occurrence of lightning. These observational studies are useful for validating modeling studies.

Recently, cloud-resolving models (CRMs) have been used to examine the role of aerosols on mixed-phase convective clouds (see Table 2). These modeling studies had many differences in terms of model configuration (2D or 3D), domain size, grid spacing (150 – 3000m), microphysics (i.e., two-moment bulk, simple or sophisticated spectral-bin), turbulence (1^{st} or 1.5 order TKE), radiation, lateral boundary conditions (i.e., closed, open and cyclic), cases (isolated convection, tropical/midlatitude squall lines) and model integration time (e.g., 2.5 to 48 hours). Almost all of the model results indicated that aerosol concentration had a significant impact on precipitation processes. For example, Khain and Pokrovsky [2004] and *Khain et al.* [2005] found that an increase in aerosol concentration (or cloud condensational nuclei, CCN) reduced precipitation processes (and rainfall) for both an East Atlantic squall line and a Texas convective cloud. They also found that an increase in CCN enhanced precipitation for an Oklahoma squall line. On the other hand, *Wang* [2005] found that precipitation could either be enhanced or reduced by increasing the CCN for a squall line that developed in the ITCZ (Intertropical Convergence Zone). *Fan et al.* [2007] found that ice microphysics, clouds and precipitation changed considerably with aerosol chemical properties for a convective event in Houston, Texas. *Fridlind et al.* [2004] found

mid-tropospheric aerosols were important as subtropical anvil nuclei for an isolated cloud, but *Khain and Porovsky* [2004] indicated that lower-tropospheric aerosols (penetrating cloud base and below 4-km) dominated for deep convective clouds. These differences could be due to model physics, cases and/or set-ups (e.g., domain size, lateral boundary conditions). *Teller and Levin* [2006] showed that high CCN concentrations reduced precipitation in mixed-phase convective clouds. Regional-scale models with fine resolution (3 km) have also been used to study the impact of aerosols on precipitation. For example, *Lynn et al.* [2005] found a "continental" aerosol concentration produces a larger earlier maximum rainfall rate than does a "maritime" aerosol concentration; however, time accumulated rain is larger with a maritime aerosol concentration. *Cheng et al.* [2006] found that increasing aerosols inhibited precipitation for an Oklahoma warm cloud system. *Van den Heever et al.* [2006] found that high-GCCN (giant CCN) and –IN (ice nuclei) cases initially enhance the surface precipitation during the first 6-hour of integration due to initial broadening of the cloud droplet spectra, whereas high CCN reduce total accumulated precipitation.

In almost all cases, idealized aerosol concentrations[1] were used in the model simulations. Furthermore, almost none of these CRM studies compared the model results with observed cloud structures, organization, radar reflectivity and rainfall. Some of the CRM domains were too small to resolve the observed clouds or precipitation systems (the domain size has to be at least twice as large as the simulated features).

This paper will investigate the effect of atmospheric aerosols on precipitation processes using a two-dimensional (2D) CRM with detailed spectral-bin microphysics. Three different cloud systems with very different environmental conditions will be simulated. Sensitivity tests will be conducted to examine the precipitation processes associated with dirty and clean environments. The model and three cases will be described in section 2. The results and comparison with previous modeling studies will be discussed in sections 3 and 4, respectively. In section 5, the summary and future work will be presented.

2. Model and Cases

2.1 Model description

The model used in this study is the 2D version of the Goddard Cumulus Ensemble (GCE) model. The GCE model was originally developed by *Soong and Ogura* [1980] and *Soong and Tao* [1980]. The equations that govern the cloud-scale motion are anelastic by filtering out sound waves. The subgrid-scale turbulence used in the model is based on *Klemp and Wilhelmson* [1978]. In their approach, one prognostic equation is solved for subgrid kinetic energy, which is then used to specify the eddy coefficients. The effect of condensation on the generation of subgrid-scale kinetic energy is also incorporated to the model [*Soong and Ogura*, 1980]. The model includes interactive solar [*Chou et al.*, 1998] and thermal infrared [*Chou and Suarez,* 1994] radiation parameterization schemes. All scalar

---

[1] Aerosol concentrations observed/measured from a previous day were used in *Fridlind et al.* [2004]. Observed cloud structure and rainfall were used for comparison in *Fan et al.* [2007].

variables (potential temperature, mixing ratio of water vapor, turbulence coefficients, and all five hydrometeor classes) use forward time differencing and a positive definite advection scheme with a non-oscillatory option [*Smolarkiewicz and Grabowski,* 1990]. The dynamic variables, u and w, use a fourth-order accurate advection scheme and leapfrog time integration. Details of the GCE model description and improvements can be found in *Tao and Simpson* [1993] and *Tao et al.* [2003].

The spectral-bin microphysics used in the GCE model were developed by *Khain et al.* [2000], *Khain et al.* [2004], and *Khain et al.* [2005]. The formulation is based on solving stochastic kinetic equations for the size distribution functions of water droplets (cloud droplets and raindrops), and six types of ice particles: pristine ice crystals (columnar and plate-like), snow (dendrites and aggregates), graupel, and frozen drops/hail. Each type is described by a size distribution using 33 categories (mass bins). Size spectra of atmospheric aerosols are also described using 33 bins.

The spectral bin microphysics includes the following processes: (1) nucleation of droplets and ice particles [*Pruppacher and Klett,* 1997; *Meyers et al.,* 1992], (2) immersion freezing [*Vali,* 1994], (3) ice multiplication [*Hallett and Mossop,* 1974; *Mossop and Hallett,* 1974], (4) detailed meltin [*Khain et al.,* 2004], (5) condensation/evaporation of liquid drops [*Pruppacher and Klett,* 1997; *Khain et al.,* 2000], (6) deposition/sublimation of ice particles [*Pruppacher and Klett,* 1997; *Khain et al.,* 2000], (7) drop/drop, drop/ice, and ice/ice collision/coalescence [*Pruppacher and Klett,* 1997; *Pinsky et al.,* 2001], (8) turbulence

effects on liquid drop collisions [*Pinsky et al.*, 2000], and (9) collisional breakup [*Seifert et al.*, 2005]. Sedimentation of liquid and ice particles is also considered. This model is specially designed to take into account the effect of atmospheric aerosols on cloud development and precipitation formation. The activation of aerosols in each size bin are explicitly calculated in this scheme [*Pruppacher and Klett*, 1997].

The initial aerosol size distribution is calculated with an empirical formula: $N = N_0 S_w^k$ [*Pruppacher and Klett*, 1997], where S_w is the super-saturation with respect to water and N_0 and k are constants. The formula gives the size distribution of the initial CCN spectrum. In this study, the baseline simulations (clean scenarios) use N_0=100 cm^{-3} and k=0.42 for the maritime case, and N_0=600 cm^{-3} and k=0.3 for the continental cases [*Twomey and Wojciechowski*, 1969]. The dirty scenarios for both the maritime and continental cases assume N_0=2500 cm^{-3} and k=0.3. In continental cases, aerosols with diameters larger than 0.8 μm are removed [*Cooper et al.*, 1997]. The oceanic aerosols have plenty of large size aerosols generated from sea spray, but they do not have very fine particles [*Hudson, 1984; Husdson, 1993*]. Therefore, small CCN, which can only be activated when the ambient super saturation exceeds 1.1% are eliminated from the maritime aerosol spectra.

Open lateral boundaries are used. At the top of the model, a free-slip condition is used for horizontal wind, temperature, and specific humidity, and zero vertical velocity is applied. There are1024 horizontal grid points with a resolution of 1 km in the center 720 points and stretched grids on either side. Use of the stretched horizontal grid makes the model less

sensitive to the choice of gravity wave speed associated with the open lateral boundary conditions [*Fovell and Ogura,* 1988]. For the present study, a stretched vertical coordinate with 33 levels is used. The model has finer resolution (about 80 meters) in the boundary layer and coarser resolution (about 1000 meters) in the upper levels. The model time step is 5 s.

2.2 Cases

Three cases, a tropical oceanic squall system observed during TOGA COARE (*Tropical Ocean and Global Atmosphere Coupled Ocean-Atmosphere Response Experiment,* which occurred over the Pacific Ocean warm pool from November 1992 to February 1993), a midlatitude continental squall system observed during PRESTORM (*Preliminary Regional Experiment for STORM-Central,* which occurred in Kansas and Oklahoma during May-June 1985), and mid-afternoon convection observed during CRYSTAL-FACE (Cirrus Regional Study of Tropical Anvils and Cirrus Layers – Florida Area Cumulus Experiment, which occurred in Florida during July 2002), will be used to examine the impact of aerosols on deep, precipitating systems. The 10-11 June 1985 PRESTORM case has been well studied [e.g., *Johnson and Hamilton,* 1988; *Rutledge et al.,* 1988; *Tao et al.,* 1995, 1996; *Lang et al.,* 2003]. The PRESTORM environment is fairly unstable and relatively dry. The model is initialized with a single sounding taken at 2330 UTC from Pratt, KS, which is ahead of the newly-forming squall line. The sounding has a lifted index of -5.37 and a convective available potential energy (CAPE) of 2300 J/kg. Radiation is included but not surface fluxes. The convective system is initiated using a low-level cold pool.

The 22 February 1993 TOGA COARE squall line has also been well studied [*Jorgensen et al.*, 1997; *Redelsperger et al.*, 2000; *Trier et al.*, 1996, 1997; *Wang et al.*, 1996, 2003]. The sounding used to initialize the model is from *LeMone et al.* [1994]. It is a composite of aircraft data below 6 km and an average of the 1800 and 2400 UTC Honiara soundings above 6 km. The CAPE and lifted index are moderately unstable, 1776 J/kg and -3.2, respectively. Surface fluxes are included in the model for this case using the TOGA COARE flux algorithm [*Fairall et al.*, 1996; *Wang et al.*, 1996]. The vertical grids are similar to the PRESTORM setup, but with the first grid of 40 m to accommodate the TOGA COARE flux algorithm. The horizontal grids follow that of PRESTORM, but with an inner resolution of 750 m. Radiation is included, and a low-level cold pool is used to start the system. Low-level mesoscale lifting is also applied. It has a peak value of 3.4 cm/s near 1 km and is applied over the first 2 hours.

Both the TOGA COARE and PRESTORM cases are well-organized and long-lived mesoscale convective systems. The CRYSTAL-FACE case is a sea breeze convection that developed over South Florida [*Ridley et al.*, 2004; *Heymsfiedl et al.*, 2004]. It originated near the coast and propagated inland and dissipated within a couple of hours. This storm generated a large anvil and had good aircraft measurements in terms of cloud chemistry. The CAPE and total precipitable water are 2027 J/kg and 4.753 g/cm^2, respectively, which are lower and more moist than the PRESTORM case but higher and drier than the TOGA COARE case. The local sounding and wind profile taken previous to the onset of convection at 1731 UTC is used in this simulation. The convection is initialized using three warm

bubbles 40 km apart with a maximum temperature perturbation of 6 K and water vapor perturbation of 6 g/kg. The rest of the model setup and physics are the same as the PRESTORM case. Table 3 shows some characteristics of the environmental conditions associated with these three cases.

3. Results

Figure 1 shows the observed and simulated radar reflectivity for the TOGA COARE, PRESTORM and CRYSTAL-FACE cases with dirty and clean conditions. The model simulations capture the various storm sizes and structures in the different environmental conditions quite well. For example, the leading convection and the extensive trailing stratiform rain area compare well with the radar reflectivity observed during the mature stage of the continental PRESTORM case [*Rutlege et al.,* 1988]. Clean cases (i.e., the control experiments) generally agree better with the observations. In terms of radar reflectivity magnitudes, the agreement between the simulations and observations is better at lower levels where only liquid phase cloud/rain water exists. The simulated radar reflectivity tends to be higher at upper levels and in the anvil area where ice phase particles dominate. This is partly due to the simplified assumption of uniform snow densities in this calculation. The melting band signal is also amplified by assuming that all of the melting particles are coated by a layer of water on their surfaces.

Figure 2 shows time sequences of the GCE model-estimated domain mean surface rainfall rate for the PRESTORM, TOGA COARE and CRYSTAL cases. Rain suppression in the high CCN concentration (i.e., dirty environment) runs is evident in all three case studies but only during the first hour of the simulations. Rain reaches the ground early in all the clean cases. This is in good agreement with observations [e.g., *Rosenfeld,* 1999, 2000]. During the mature stage of the simulations, the effect of increasing the CCN concentration ranges from rain suppression in the PRESTORM case to little effect in the CRYSTAL-FACE case to rain enhancement in the TOGA COARE case. These results suggest that long-term model simulations are needed in order to assess the impact of aerosols on precipitation processes associated with mesoscale convective systems and thunderstorms. These results also show the complexity of aerosol-cloud-precipitation interaction within deep convection.

Table 4 shows the domain-averaged surface rainfall amounts, stratiform percentages, precipitation efficiencies, and ice water path ratios (ice water path divided by the sum of the liquid and ice water paths) for the TOGA COARE, PRESTORM and CRYSTAL-FACE cases under clean and dirty conditions. The precipitation is divided into convective and stratiform components [*Tao et al.,* 1993; *Lang et al.,* 2003]. The convective region includes areas with strong vertical velocities (over 3-5 m s^{-1}) and/or heavy surface rainfall. The stratifrom region is simply non-convective. For the PRESTORM case, the dirty scenario produces more stratiform (light) precipitation than does the clean case. It is expected that a high CCN concentration allows for more small cloud droplets and ice particles to form. The lower collection coefficient for smaller cloud and ice particles allows for a larger amount of

ice phase particles to be transported into the trailing stratiform region, producing a higher stratiform rain percentage in the dirty case. Aerosols do not have much impact on the straiform percentage for the CRYSTAL-FACE case because of its short life span. The reduction in stratiform rain (or light rain) in the dirty environment for the TOGA COARE case is due to its enhanced convective activity (stronger updrafts).

Precipitation efficiency (PE) is an important physical parameter for measuring the interaction between convection and its environment. Its definition varies [e.g., *Ferrier et al.*, 1996; *Sui et al.*, 2007]. In this study, the precipitation efficiency is defined as PE = (P - L) / P, where P is the total mass of hydrometeors formed in clouds by diffusional growth, and L is the loss of hydrometeor mass due to drop evaporation and ice sublimation. When total evaporation and sublimation are very small, PE will be close to 1. Smaller PE generally indicates more evaporation/sublimation (i.e., during the decaying or less active stage of clouds/cloud systems). The PEs of cloud systems in drier environments (e.g., PRESTORM and CRYSTAL-FACE) are generally smaller than those in moist environments (e.g., TOGA COARE). In addition, the simulations with a dirty environment have a smaller PE than their counterparts for all three cases. This is because the smaller cloud droplets/ice particles simulated in the dirty cases result in larger evaporation/sublimation. Table 4 also shows higher ice water path ratios for the continental cloud systems (i.e., PRESTORM and CRYSTAL-FACE). The larger CAPE and stronger convective updrafts in the PRESTORM and CRYSTAL-FACE produce more ice particles than in the TOGA COARE case.

For the PRESTORM and CRYSTAL-FACE cases, the PE in the dirty run is only 7% and 5% smaller, respectively, than in the clean run. The strengths of the convective updrafts vary little between the dirty and clean scenarios for both cases (Fig. 3). This could be the reason for the small changes in PE between the dirty and clean runs and could also account for the similarity in their ice water paths. The PE is reduced by 13% in the dirty scenario for the TOGA COARE case. The much stronger convective activity simulated in the dirty case produces larger anvil and more ice sublimation. This may be the cause of smaller PE in the dirty case. This also shows that the dirty environment leads to more ice formation for TOGA COARE.

Figure 3 shows time sequences of GCE model-simulated maximum vertical velocity for PRESTORM, TOGA COARE and CRYSTAL-FACE. The maximum vertical velocity is stronger in PRESTORM than in both TOGA COARE and CRYSTAL because PRESTORM has the largest CAPE. *Williams et al.* [2002] suggested that updraft strength would be stronger in a dirty environment. For both PRESTORM and CRYSTAL, the maximum vertical velocity for the dirty scenario is slightly stronger than the clean environment during the early stages of storm development. However, aerosols do not have a major influence on the maximum vertical velocities in these two continental cases. The TOGA COARE case, on the other hand, shows much stronger maximum vertical velocities with a high CCN concentration (dirty environment). This is consistent with the increase in simulated surface precipitation. The maximum vertical velocities do not vary between the dirty and clean runs in the early stages of the TOGA COARE case.

Figure 4 shows probability distribution functions (PDFs) of rainfall intensity for the PRESTORM, TOGA COARE and CRYSTAL cases during the first hour of simulation. All three cases produce more light rain in the dirty environment. This result is in good agreement with observations [*i.e., Rosenfeld and Ulbrich,* 2003]. However, over the entire 9-hour simulation, only the PRESTORM case maintains this characteristic. In TOGA COARE, more light precipitation was simulated in the clean case, contrary to the first hour results, because simulated vertical velocities are weaker with a low CCN. The cumulated surface rainfall PDFs for the clean and dirty scenarios do not differ significantly over the 5-hour storm duration in CRYSTAL.

Rosenfeld and Lensky [1998] suggested that a deeper mixed-phase layer may exist in dirty environments (high CCN). *Williams et al.* [2002] and *Andreae et al.* [2004] also suggested that higher maximum lightning flash rates associated with more mixed phase processes would occur for dirty environments. In this study, additional model sensitivity experiments were performed by turning off the ice processes to examine the impact of ice microphysics on the aerosol-precipitation interactions. Figure 5 shows time sequences of GCE model-estimated domain mean surface rainfall rate without ice processes (warm rain only). For the PRESTORM case, the mean surface rainfall under both clean and dirty conditions is quite similar. The establishment of steady rain is also much faster compared with the full ice runs. This suggests that the ice processes are crucial in suppressing surface precipitation and increasing the portion of light rain in a dirty environment. For TOGA

COARE, rain suppression due to high CCN is again only evident during the first hour of the simulations. For the entire period, increasing CCN still enhances rainfall; the same as with the full ice run. These results suggest that ice processes do not have a major impact on the aerosol-precipitation interactions for the TOGA COARE case, because the majority of surface rainfall in this case comes from warm rain. Evaporative cooling and the strength of the cold pool, which affect cell regeneration in squall systems, are determined mainly by warm rain processes for the TOGA COARE case. Therefore, the ice processes can only play a secondary role in terms of aerosol-precipitation interactions. For the CRYSTAL case, rainfall is enhanced with a high CCN. This enhancement is mainly associated with a relatively strong new cell generated at around t=2.5 hours. This may be caused by the enhanced rain evaporation associated with the dirty case. These sensitivity tests also show the complexity of aerosol-precipitation interactions in mixed-phase, deep convection.

Figure 6 shows the integrated total water and ice paths averaged every hour for clean and dirty conditions. The portions due to cloud water and pristine ice content are shown in hatched lines. For the PRESTORM case, the ice path is much larger than the liquid water path. More ice particles are produced by this convective system when a high CCN is assumed. However, the liquid water path is generally reduced with high CCN because smaller cloud particles have less chance of being collected. Instead, more of them are transported above the freezing level and subsequently become ice particles in the dirty scenario. This is also why less rainfall reaches the ground for the high CCN scenario in PRESTORM. For the TOGA COARE case, both liquid water path and ice water path

increase when a high CCN is assumed. This is consistent with the more vigorous convection simulated in the dirty run. The ice path is still much smaller in this case than in the PRESTORM case. This is why the TOGA COARE case is less sensitive to ice processes compared with the PRESTORM case. More ice particles are also produced when a high CCN is assumed for the CRYSTAL-FACE case, but the differences are relatively small. As with the TOGA COARE case, the ice paths in CRYSTAL-FACE are much smaller than in the PRESTORM case. However, ice is produced at a very early stage in CRYSTAL-FACE as compared to TOGA COARE. This is why the CRYSTAL case is sensitive to ice processes.

During the initial stages of cloud formation (the first hour), cloud water dominates the total liquid water path for the dirty runs, in contrast to the considerable amounts of rain water in the clean runs. This again shows that rain formation is suppressed by increasing aerosols. However, this suppression becomes less obvious once the precipitation is well established, especially for the long-lived squall systems in PRESTORM and TOGA COARE.

Figure 7 shows a schematic diagram of the physical processes that cause either enhancement (TOGA COARE) or suppression (PRESTORM) of precipitation in a dirty environment. In the early developing stages, small cloud droplets are produced in both the TOGA COARE and the PRESTORM cases with high CCN. Both cases also show narrower cloud drop size spectra for high CCN (not shown). This result is in good agreement with observations [i. e., *Twomey et al.,* 1984; *Albrecht,* 1989; *Rosenfeld,* 1999]. In this early

stage, rain is suppressed for both cases with high CCN, which is also in good agreement with observations [*e.g., Rosenfeld,* 1999, 2000]. The suppression of precipitation in dirty conditions is mainly due to microphysical processes only. Smaller cloud droplets collide/coalesce less efficiently, delaying raindrop formation. These processes are important especially in the early/developing stage of a cloud system.

The smaller cloud droplets simulated in the dirty cases evaporate faster than in the clean cases. The near surface cold pool strength could thus be enhanced by stronger evaporative cooling. When the cold pool interacts with the lower level wind shear, the convergence could become stronger, producing stronger secondary convection for the dirty cases. This can lead to more vigorous precipitation processes and enhanced surface precipitation. These processes seem to be occurring in the TOGA COARE case, as shown in Fig. 8b. In this case, evaporative cooling is more than twice as strong in the lower troposphere for the dirty scenario compared to the clean scenario. On the other hand, evaporative cooling is stronger at lower levels in the clean scenario for the PRESTORM case. This is related to the heavier and early onset of rainfall in that run and because rain evaporation dominates the lower levels. At higher levels in the PRESTORM case, cloud evaporation is still stronger for the dirty case as shown in Fig. 8a.

For all three cases, the dirty scenarios produce smaller cloud droplets with narrower spectrum, a delayed onset of rainfall, increased duration of diffusional droplet growth, increased latent heat release above the freezing level, and stronger vertical velocities at

higher altitudes. The higher cloud tops, stronger updrafts, and deeper mixed-phase regions simulated in the dirty runs are in good agreement with observations (Table 1). The simulations all show that when the air is polluted, convection produces more ice particles, which is also in good agreement with observations. This is potentially important for the formation and maintenance of high altitude ice clouds in the anvil area, which in turn may play an important role in the Earth's radiation budget.

4. Comparison with Previous Modeling Studies

Previous modeling studies have examined the role of aerosols on mixed-phase convective clouds for particular cases with different sets of model configurations and microphysics schemes (see Table 2). Although most of the model settings in those studies are not technically equivalent to this study, it is yet worthwhile to compare and review the different results. A simple metric, changes in time-integrated precipitation ($dP = 100 * (P_{dirty} - P_{clean}) / P_{clean}$) as a result of increases in the number concentration of CCN ($dN_0 = N_{dirty} - N_{clean}$), is used to examine the different studies (Table 5).

Phillips et al. [2002] is one of the earliest studies that applied an explicit microphysics module with a 2D CRM to examine the influence of aerosol concentrations on a summer-time cumulus cloud over New Mexico. The coupling is one-way (i.e., the CRM provides dynamic input to the microphysics module). For a shallow cumulus (about 5 km cloud top), *Phillips et al.* [2002] found that with increased CCN, the precipitation rate, warm-rain production, and secondary ice production are reduced. Although the sensitivity of ice

microphysics to the aerosol number concentration appeared to be much less for the deep-convective scenario than for the shallow-convective cases, increasing the CCN from super-maritime (N_0=800) to control (N_0=2750) and super-continental (N_0=5000) scenarios decreased the accumulated precipitation by 14% and 30%, respectively. In addition, the onset of precipitation is delayed by about 5 and 15 minutes, respectively, for the high CCN scenarios in comparison with the low CCN scenario.

Khain and Pokrovsky [2004] and *Khain et al.* [2005] used a 2D CRM with spectral microphysics (the same microphysics as used in this paper) to examine the aerosol impact on three deep convective clouds: an Atlantic squall line, an Oklahoma squall line (the same PRESTORM case in this paper), and a Texas convective cloud. Their results indicated that high CCN concentrations enhanced the precipitation processes for the Atlantic and Oklahoma squall line cases, but suppressed them for the Texas convective cloud. The results from *Khain and Pokrovsky* [2004] and *Khain et al.* [2005] also showed that high CCN could delay the warm-rain process and enhance cold-rain processes for all three cases. These features are also simulated in the present study. For cases having suppressed precipitation with high CCN (the Texas convective cloud), a higher sublimation of ice and evaporation of drops (evaporative cooling) resulted in a higher loss of precipitation mass. The PRESTORM case simulated in this present paper also showed larger evaporative cooling with higher CCN. For cases having enhanced precipitation with high CCN (the Atlantic and Oklahoma squall lines), stronger updrafts/downdrafts and stronger convergence in the boundary layer may have enhanced the triggering of secondary clouds and produced a longer lifetime for the

convective system. Stronger updrafts and downdrafts are also simulated in the current TOGA COARE case with high CCN. However, there is a major difference between their study and this one for the PRESTORM case. While their results showed enhanced precipitation (dP=258%) for the PRESTORM case, the current results show suppression of precipitation with high CCN. They also simulated a short-lived squall line for the case with low CCN. The different domain sizes used in the two studies could cause the difference. This study had a larger horizontal domain than did *Khain et al.* [2004, 2005] in order to simulate the large convective system and minimize the reflection of convectively-generated gravity waves at the lateral boundaries [*Fovell and Ogura,* 1988].

Teller and Levin [2006] used a 2D CRM with spectral microphysics [*Reisin et al.,* 1998] to examine the aerosol impact on a winter convective cloud in the eastern Mediterranean region. Their results also showed that high CCN could delay rainfall and enhance cold rain processes. Their results also showed that larger number concentrations of CCN can decrease accumulated precipitation by 27% ~ 93% over 80-minute model integration. These features are also simulated in the present PRESTORM and CRYSTAL cases. They also found that an increase in IN could reduce the total amount of precipitation but GCCN could enhance total precipitation in polluted clouds.

Wang [2005] used a 3D CRM with a two-moment bulk microphysical scheme to examine the aerosol impact on a convective system that developed in the ITCZ. His results showed that a high initial CCN concentration could produce stronger convection, more condensed cloud water mass, enhanced microphysical conversions, and more surface rainfall.

Wang [2005] indicated that there are three processes by which precipitation is increased in tropical deep convection due to high CCN: (1) enhanced convective strength due to stronger and more latent heat release; (2) the dominant role of ice phase microphysics in rain production; and (3) greatly increased total water content in small liquid particles. The current tropical oceanic case (TOGA COARE) also produces stronger updrafts through more latent heat release. However, ice processes are not the dominant processes for rain production (see the sensitivity test shown in Fig. 5b). Differing dimensionalities, microphysical schemes, lateral boundary conditions, and tropical cases (initial conditions) could explain the differences between the model results.

Lynn et al. [2005] used spectral-bin microphysics (a simplified version of Khain's scheme [*Khain et al.*, 2004]) and the fifth-generation Pennsylvania State University-National Center for Atmospheric Research (Penn State-NCAR) Mesoscale Model (MM5) to simulate a cloud that approached the west coast of Florida, prior to the sea-breeze development on 27 July 1991. The use of a continental CCN concentration led to a delay in the growth of rainfall (in agreement with the present modeling study). Their results show that a continental CCN concentration can reduce cumulative precipitation by 5% versus a maritime one.

Van den Heever et al. [2006] used the Regional Atmospheric Modeling System (RAMS) and a two-moment bulk microphysical scheme [*Meyers et al.*, 1997; *Saleeby and Cotton*, 2004] to examine the aerosol effect on the formation of a thunderstorm over the peninsula of Florida (28 July 2002 during CRYSTAL-FACE). Sensitivity studies show that

different combinations of CCN, GCCN, and IN result in different amounts and temporal patterns of cloud-water/ice contents and rainfall. Their study showed that high CCN reduce cumulative precipitation by 22% compared to low CCN. In addition, high-GCCN and IN enhanced surface precipitation for the first 6 hours of integration due to the initial broadening of the cloud droplet spectra. However, the total (12-hour integration) accumulated precipitation was greatest for the clean (low CCN, GCCN, and IN) case. This could be explained by a rapid wet deposition of GCCN for the first 6 hours of integration. All their experiments involving high CCN resulted in high cloud-water content and weak surface precipitation.

Among these previous studies, the most striking difference is that cumulative precipitation can either increase or decrease in response to higher concentrations of CCN. *Khain and Pokrovsky* [2004] and *Teller and Levin* [2006] changed the number concentrations of CCN gradually and found robust decreases in cumulative precipitation for higher concentrations of CCN (Table 5). This is completely opposite from the result in *Wang* [2005]. Understanding these discrepancies is a necessary next step in resolving aerosol effects on cloud microphysics, dynamics and precipitation within climate systems.

5. Summary and Future Work

A 2D CRM with detailed spectral-bin microphysics is used to examine the aerosol impact on deep convective clouds. Three cases are simulated using idealized initial aerosol concentrations: a case of sea breeze convection in Florida during CRYSTAL-FACE, a

tropical mesosocale convective system during TOGA COARE, and a summertime midlatitude squall line during PRESTORM. Comparisons between the model simulations and in situ radar reflectivity observations show good agreements. A pair of model simulations, an experiment with low (clean) and an experiment with high CCN (dirty environment), is conducted for each case. The major highlights are as follows:

- For all three cases, higher CCN produces smaller cloud droplets and a narrower spectrum. Dirty conditions delay rain formation, increase latent heat release above the freezing level, and enhance vertical velocities at higher altitude for all cases. Stronger updrafts, deeper mixed-phase regions, and more ice particles are simulated with higher CCN in good agreement with observations.
- In all cases, rain reaches the ground early with lower CCN. Rain suppression is also evident in all three cases with high CCN in good agreement with observations *(Rosenfeld,* 1999, 2000 and others). Rain suppression, however, only occurs during the first hour of simulation.
- During the mature stage of the simulations, the effect of increasing aerosol concentration ranges from rain suppression in the PRESTORM case to little effect on surface rainfall in the CRYSTAL-FACE case to rain enhancement in the TOGA COARE case.
- The model results suggest that evaporative cooling is a key process in determining whether higher CCN reduces or enhances precipitation. Cold pool strength can be enhanced by stronger evaporation. When cold pool interacts with the near surface wind shear, the low-level convergence can be stronger, facilitating secondary cloud formation

and more vigorous precipitation processes. The smaller cloud droplets simulated with high CCN generally evaporate faster than the larger droplets simulated with low CCN. Evaporative cooling is more than two times stronger at low levels with higher CCN for the TOGA COARE case. However, evaporative cooling is slightly stronger at lower levels with lower CCN for the PRESTORM case. PRESTORM has a very dry environment and both large and small rain droplets can evaporate. Consequently, the cold pool is weaker, and the system is less intense with higher CCN.

- Sensitivity tests are conducted to determine the impact of ice processes on aerosol-precipitation interaction. The results suggested that ice processes are crucial for suppressing precipitation due to high CCN for the PRESTORM case. More and smaller ice particles are generated in the dirty case and transported to the trailing stratiform region. This reduces the heavy convective rain and contributes to the weakening of the cold pool. Warm rain processes dominate the TOGA COARE case. Therefore, ice processes only play a secondary role in terms of aerosol-precipitation interaction.
- Two of the three cloud systems presented in this paper formed a line structure (squall system). A 2D simulation, therefore, gives a good approximation to such a line of convective clouds. Since the real atmosphere is 3D, further 3D cloud-resolving simulations are needed to address aerosol-precipitation interactions.

Most previous modeling results found that high CCN concentrations could suppress precipitation processes (i.e., *Khain et al.,* 2004, 2005; *Cheng et al.,* 2006, *Lynn et al.,* 2005; *Van den Heever et al.,* 2006; *Teller and Levin,* 2006). However, high CCN concentrations

could also enhance precipitation processes (Wang 2005; Khain *et al.* 2005). These results show the complexity of aerosol interactions with convection. More case studies are required to further investigate the aerosol impact on rain events. In almost all previous cloud-resolving modeling studies (including the present study), idealized CCN concentrations were used in the model simulations. A horizontally uniform distribution of CCN was also used in the mesoscale modeling studies. A non-homogeneous CCN distribution, consistent with the non-homogeneous initial meteorological conditions, will be required to assess aerosol-precipitation interactions using regional-scale models in the future. In addition to IN and GCCN, the chemistry of CCN needs to be considered in future modeling of aerosol-precipitation interactions.

Many previous CRM studies did not compare model results with observed cloud structures, organization, radar reflectivity and rainfall. Some of the CRM domains were too small to resolve the observed clouds or precipitation systems (the domain size has to be at least twice as large as the simulated features). It may require major field campaigns to gather the data necessary to both initialize (with meteorological and aerosol) and validate (i.e., in situ cloud property observations, radar, lidar, and microwave remote sensing) the models. Although CRM-simulated results can provide valuable quantitative estimates of the indirect effects of aerosols, CRMs are not global models and can only simulate clouds and cloud systems over a relatively small domain. Close collaboration between the global and CRM communities is needed in order to expand the CRM results to a regional and global perspective.

Acknowledgment

The GCE model is mainly supported by the NASA Headquarters Atmospheric Dynamics and Thermodynamics Program and the NASA Tropical Rainfall Measuring Mission (TRMM). The authors are grateful to Dr. R. Kakar at NASA headquarters for his support of this research. The authors acknowledge NASA Goddard Space Flight Center for computer time used in this research.

The research was also supported by the Office of Science (BER), U. S. Department of Energy/Atmospheric Radiation Measurement (DOE/ARM) Interagency Agreement No. DE-AI02-04ER63755. The authors are grateful to Dr. Kiran Alapaty at DOE/ARM for his support of this research.

References

Ackerman, A. S., O. B. Toon, D. E. Stevens, A. J. Heymsfield, V. Ramanathan and E. J. Welton (2000), Reduction of tropical cloudiness by soot, *Science*, *288*,1042-1047.

Albrecht, B. A. (1989), Aerosols, cloud microphysics and fractional cloudiness, *Science*, *245*, 1227-1230.

Andreae M. O., D. Rosenfeld, P. Artaxo, A. A. Costa, G. P. Frank, K. M. Longo, and M. A. F. Silva-Dias (2004), Smoking rain clouds over the Amazon, *Science*, *303*(5662), 1337–1342.

Bell, T. L., D. Rosenfeld, K.-M. Kim, J.-M. Yoo, M.-I. Lee, and M. Hahnenberger (2007), Midweek increase in U.S. Summer rain and storm heights suggests air pollution invigorates rainstorms, *J. Geophys. Res.*, (submitted).

Cheng, C.-T., W.-C. Wang, and J.-P. Chen (2006), A modeling study of aerosol impacts on cloud microphysics and radiative properties, *Q. J. R. Meteorol. Soc.*, (accepted).

Chou, M.-D., and M. J. Suarez (1994), An efficient thermal infrared radiation parameterization for use in general circulation models. *NASA Tech. Memo. 104606, 85pp.*

Chou, M.-D., M. J. Suarez, C.-H. Ho, M.-H. Yan, and K.-T. Lee (1998), Parameterizations for Cloud Overlapping and Shortwave Single-Scattering Properties for Use in General Circulation and Cloud Ensemble Models, *J. Clim,, 11,* 202-214.

Cooper, W. A., Bruintjes, R., Mather, G. (1997), Calculations pertaining to hygroscopic seeding with flares, *J. Appl. Meteorol., 36*, 1449-1469.

Fairall, C. W., E. F. Bradley, D. P. Rogers, J. B. Edson, and G. S. Young (1996), Bulk parameterization of air-sea fluxes for Tropical Ocean Global Atmosphere Coupled Ocean-Atmosphere Response Experiment, *J. Geophys. Res., 101,* 915-929.

Fan, J, R. Zhang, G. Li, W.-K. Tao, and X. Li (2007), Simulation of cumulus clouds using a spectral microphysics cloud-resolving model, *J. Geophys. Res., 112, D04201,* doi:10.1029/2006JD007688.

Ferrier, B. S., J. Simpson, and W.-K. Tao (1996), Factors responsible for precipitation efficiencies in midlatitude and tropical squall simulations. *Mon. Wea. Rev., 124,* 2100-2125.

Fovell, R. G, and Y. Ogura (1988), Numerical simulation of a midlatitude squall line in two dimensions. *J. Atmos. Sci., 45,* 3846-3879.

Fridlind, A. M., and co-authors (2004), Evidence for the predominance of mid-tropospheric aerosols as subtropical anvil cloud nuclei, *Science, 304,* 718-722.

Hallet, J., and S. C. Mossop (1974), Production of secondary ice crystals during the riming process, *Nature, 249,* 26-28.

Heymsfield, G. M., A. J. Heymsfield and L. Belcher (2004), Observations of Florida convective storms using dual wavelength airborne radar. *International Conf. on Clouds and Precipitations.* Bologna, Italy, 18-23 July 2004.

Hudson, J. G. (1984), Cloud condensation nuclei measurements within clouds, *J. Clim. Appl. Meteorol., 23,* 42-51.

Hudson, J. G. (1993), Cloud condensation nuclei near marine cumulus, *J. Geophys. Res., 98,* 2693-2701.

Johnson, R. H., and P. J. Hamilton (1988), The relationship of surface pressure features to the precipitation and airflow structure of an intense midlatitude squall line, *Mon. Wea. Rev., 116,* 1444-1472.

Jorgensen, D. P., M. A. LeMone, and S. B. Trier (1997), Structure and evolution of the 22 February 1993 TOGA COARE squall line: Aircraft observations of precipitation, circulation, and surface fluxes. *J. Atmos. Sci., 54,* 1961-1985.

Khain, A., A. Pokrovsky, and I. Sednev (1999), Some effects of cloud-aerosol interaction on cloud microphysics structure and precipitation formation: Numerical experiments with a spectral microphysics cloud ensemble model. *Atmos. Res., 52,* 195-220.

Khain, A., M. Ovtchinnikov, M. Pinsky, A. Podrovsky, and H. Krugliak (2000), Notes on the state-of-art numerical modeling of cloud microphysics, *Atmos. Res., 55,* 159-224.

Khain, A., A. Pokrovsky, M. Pinsky, A. Seigert, and V. Phillips (2004), Simulation of effects of atmospheric aerosols on deep turbulent convective clouds using a spectral microphysics mixed-phase cumulus cloud model. Part I: Model description and possible applications. *J. Atmos. Sci., 61,* 2983-3001.

Khain, A., and A. Pokrovsky (2004), Simulation of effects of atmospheric aerosols on deep turbulent convective clouds using a spectral microphysics mixed-phase cumulus cloud model. Part II: Sensitivity study. *J. Atmos. Sci., 61,* 2963-2982.

Khain, A., D. Roseenfeld, and A. Pokrovsky (2005), Aerosol impact on the dynamics and microphysics of deep convective clouds. *Q. J. R. Meteorol. Soc., 131*, 1-25.

Klemp, J. B., and R. B. Wilhelmson (1978), The simulation of three-dimentional convective storm dynamics. *J. Atmos. Sci., 35,* 1070-1096.

Koren, I., Y. J. Kaufman, D. Rosenfeld, L. A. Remer, and Y. Rudich (2005), Aerosol invigoration and restructuring of Atlantic convective clouds, *Geophys. Res. Lett., 32,* L14828, doi:10.1029/2005GL023187.

Lang, S., W.-K. Tao, J. Simpson, and B. Ferrier (2003), Modeling of convective-stratiform precipitation processes: Sensitivity to partitioning methods. *J. Appl. Meteor., 42,* 505-527.

LeMone, M. A., D. P. Jorgensen, and B. F. Smull (1994): The impact of two convective systems of sea surface stresses in COARE. *Preprints, Sixth Conf. On Mesoscale Processes, Portland, OR, Amer. Meteor. Soc.*, 40-44.

Linn, J. C., T. Matsui, R.A. Pielke Sr., and C. Kummerow (2006), Effects of biomass burning-derived aerosols on precipitation and clouds in the Amazon Basin: A satellite-based empirical study, *J. Geophys. Res.*, *111*, D19204, doi:10.1029/2005JD006884.

Lynn, B. H., A. Khain, J. Dudhia, D. Rosenfeld, A. Pokrovsky and A. Seifert (2005), Spectral (bin) microphysics coupled with a mesoscale model (MM5) Part II: Simulation of a CaPE rain event with a squall line, *Mon. Wea. Rev.*, *133*, 59-71.

Meyers, M. P., P. J. DeMott, and W. R. Cotton (1992), New primary ice-nucleation parameterization in an explicit cloud model. *J. App. Meteor, 31,* 708 721.

Meyers, M. P., R. L. Walko, J. Y. Harrington, and W. R. Cotton (1997), New RAMS cloud microphysics parameterization. Part II: The two-moment scheme, *Atmos. Res., 45,* 3-39.

Mossop, S. C., and J. Hallet (1974), Ice crystal concentration in cumulus clouds: influence of the drop spectrum, *Science, 186,* 632 634.

National Research Council (NRC) (2005), Radiative forcing of climate change: Expanding the concept and addressing uncertainties. Washington, D.C., The National Academies Press.

Orville, R. E., R. Zhang, J. N. Gammon, D. Collins, B. Ely, and S. Steiger (2001), Enhancement of cloud-to-ground lightening over Houston Texas. *Geophys. Res. Lett.*, 28, 2597-2600.

Phillips, V. T. J., T. W. Choularton, A. M. Blyth, and J. Latham (2002), The influence of aerosol concentrations on the glaciation and precipitation of a cumulus cloud, *Q. J. R.*

Meteorol. Soc., *128*(581), 951–971.

Pinsky, M., A. P. Khain, and M. Shapiro (2000), Stochastic effect on cloud droplet hydrodynamic interaction in a turbulent flow, *Atmos. Res.*, *53*, 131 169.

Pinsky, M., A. P. Khain, and M. Shapiro (2001), Collision efficiency of drops in a wide range of Reynolds numbers: Effects of pressure on spectrum evolution. *J. Atmos. Sci.*, *58*, 742 764.

Pruppacher, H. R., and J. D. Klett (1997), Microphysics of clouds and precipitation. 2nd edition. Oxford Press, 914pp.

Redelsperger, J.-L., and Co-authors (2000), A GCSS model intercomparison for a tropical squall line observed during TOGA-COARE. Part I: Cloud-resolving models. *Quar. J. Roy. Meteor. Soc.*, *126*, 823-863.

Ramanathan, V., P. J. Crutzen, J. T. Kiehl and D. Rosenfeld (2001), Aerosols, climate, and the hydrological cycle, *Science*, *294*, 2119-2124.

Reisin, T. G., Y. Yin, Z. Levin, and S. Tzivion (1998), Development of giant drops and high reflectivity cores in Hawaiian clouds: Numerical simulation using a kinematic model with detailed microphysics, *Atmos. Res.*, *45*, 275-297.

Ridley, B., L. Ott, K. Pickering, and 13 coauthors (2004), Florida thunderstorms: A faucet of reactive nitrogen to the upper troposphere, *J. Geophys. Res.*, *109*, D17305, doi:10.1029/2004JD004769.

Rosenfeld, D. and I. Lensky (1998), Satellite-based insights into precipitation formation processes in continental and maritime convective clouds, *Bull. Amer. Meteor. Soc. 79*, 2457- 2476.

Rosenfeld D. (1999), TRMM observed first direct evidence of smoke from forest fires inhibiting rainfall, *Geophy. Res. Lett. 26, (20),* 3105-3108.

Rosenfeld, D. (2000), Suppression of rain and snow by urban and industrial air pollution, *Science, 287,* 1793-1796.

Rosenfeld, D. and W. L. Woodley, 2000: Convective clouds with sustained highly supercooled liquid water down to –37 °C. *Nature*, **405**, 440-442.

Rosenfeld D., Y. Rudich, and R. Lahav (2001), Desert dust suppressing: A possible desertification feedback loop, *Proc. Natl. Acad. Sci., 98,* 5975–5980.

Rosenfeld D. and C. W. Ulbrich, 2003: Cloud microphysical properties, processes, and rainfall estimation opportunities. Chapter 10 of " Radar and Atmospheric Science: A Collection of Essays in Honor of David Atlas". Edited by Roger M. Wakimoto and Ramesh Srivastava. *Meteorological Monographs* **52**, 237-258, AMS.

Rutledge, S. A., R. A. Houze, Jr., and M. I. Biggerstaff (1988), The Olkahoma-Kansas mesoscale convective system of 10-11 June 1985: Precipitation structure and single-doppler radar analysis, *Mon. Wea. Rev., 116,* 1409-1430.

Seifert, A., A. Khain, U. Blahak, and K. D. Beheng (2005), Possible effects of collisional breakup on mixed-phase deep convection simulated by a spectral (bin) cloud model, *J. Atmos. Sci., 62,* 1917-1931.

Smolarkiewicz, P. K., and W. W. Grabowski (1990), The multidimensional positive advection transport algorithm: Nonoscillatory option. *J. Comput. Phys., 86,* 355 375.

Saleeby, S. M. and W. R. Cotton (2004), A large-droplet mode and prognostic number concentration of cloud droplets in the Colorado State University Regional Atmospheric

Modeling System (RAMS). Part I: module descriptions and supercell test simulations, *J. App. Meteror. 43*, 182-195.

Soong, S.-T., and Y. Ogura (1980), Response of trade wind cumuli to large-scale processes. *J. Atmos. Sci., 37,* 2035-2050.

Soog, S.-T., and W.-K. Tao (1980), Response of deep tropical clouds to mesoscale processes. *J. Atmos. Sci., 37,* 2016-2034.

Sui, C.-S., X. Li, and M.-J. Yang (2007), On the definition of precipitation efficiency. *J. Atmos. Sci.,* (accepted)

Tao, W.-K., and J. Simpson (1993), Goddard Cumulus Ensemble Model. Part I: Model description. *Terr. Atmos. Ocea. Sci., 4,* 35-72.

Tao, W.-K., J. Scala, J. Simpson (1995), The effects of melting processes on the development of a tropical and a midlatitude squall line, *J. Atmos. Sci., 52,* 1934-1948.

Tao, W.-K., S. Lang, J. Simpson, C.-H. Sui, B. Ferrier, and M.-D. Chou (1996), Mechanisms of cloud-radiation interaction in the tropics and midlatitudes, *J. Atmos. Sci., 53,* 2624-2651.

Tao, W.-K., J. Simpson, D. Baker, S. Braun, M.-D. Chou, B. Ferrier, D. Johnson, A. Khain, S. Lang, B. Lynn, C.-L. Shie, D. Starr, C.-H. Sui, Y. Wang, and P. Wetzel (2003), Microphysics, radiation and surface processes in the Goddard Cumulus Ensemble (GCE) model. *Meteorol. Atmos. Phys., 82,* 97-137.

Teller, A., and Z. Levin (2006), The effects of aerosols on precipitation and dimensions of subtropical clouds: a sensitivity study using a numerical cloud model, *Atmos. Chem. Phys.*, **6**, 67–80.

Trier, S. B., W. C. Skamarock, M. A. LeMone, D. B. Parsons, and D. P. Jorgensen (1996), Structure and evolution of the 22 February 1993 TOGA COARE squall line: Numerical simulations, *J. Atmos. Sci., 53,* 2861-2886.

Trier, S. B., W. C. Skamarock, and M. A. LeMone (1997), Structure and evolution of the 22 Februaru 1993 TOGA COARE squall line: Organization mechanisms inferred from numerical simulation, *J. Atmos. Sci., 54,* 386-407.

Twomey S., and T. A. Wojciechowski (1969), Observations of the geographical variation of cloud nuclei. *J. Atmos. Sci., 26,* 684 688.

Twomey, S. A., 1977: The influence of pollution on the shortwave albedo of clouds. *J. Atmos. Sci.*, **34**, 1149-1152.

Twomey, S. A., M. Piepgrass, and T. L. Wolfe (1984), An assessment of the impact of pollution on global cloud albedo, *Tellus, 36B,* 356-366.

Vali, G. (1994), Freezing rate due to heterogeneous nucleation. *J. Atmos. Sci., 51,* 1843 1856.

Van den Heever, S. C., G. G. Carrió, W. R. Cotton, P. J. DeMott, and A. J. Prenni (2006), Impact of nucleating aerosol on Florida storms. Part 1: mesoscale simulations, *J. Atmos. Sci., 63,* 1752-1775.

Wang, C. (2005), A model study of the response of tropical deep convection to the increase of CCN concentration. 1. Dynamics and microphysics. *J. Geophys. Res., 110,* D21211, doi:10.1029/2004JD005720.

Wang, Y., W.-K. Tao, and J. Simpson (1996): The impact of a surface layer on a TOGA COARE cloud system development. *Mon. Wea. Rev., 124,* 2753-2763.

Wang, Y., W.-K. Tao, J. Simpson, and S. Lang (2003): The sensitivity of tropical squall lines to surface fluxes: Three-dimensional cloud resolving model simulations. *Quart. J. Roy. Meteor. Soc., 129,* 987-1006.

Williams, E. D. Rosenfeld and co-authors (2002), Contrasting convective regimes over the Amazon: Implications for cloud electrification. *J. Geophys. Res., 107, D20,* 8082, doi:10.1029/2001JD000380.

Table Captions

Table 1: Key observational studies identifying the differences in the microphysical properties, cloud characteristics, thermodynamics, and dynamics associated with clouds and cloud systems developed in dirty and clean environments.

Table 2: Key papers using CRMs to study the impact of aerosols on precipitation. Model dimensionality (2D or 3D), microphysical schemes (spectral-bin or two-moment bulk), turbulence parameterization (1st or one and a half order TKE), radiation (with or without), domain size (km), resolution (m), time step (seconds), lateral boundary condition (closed, cyclic or radiative open), case and integration time (hours) are all listed.

Table 3: Initial environmental conditions expressed in terms of CAPE (convective available potential energy) and precipitable water for the TOGA COARE, PRESTORM and CRYSTAL-FACE case. The geographic locations, storm type and previous modeling papers are also shown.

Table 4: Domain-averaged surface rainfall amount (in mm day^{-1}), stratiform percentage (in %), precipitation efficiency (PE in %), and ice water path ratio (ice water path divided by the total liquid and ice water path) for the TOGA COARE, PRESTORM and CRYSTAL-FACE case under dirty and clean conditions. Note there are 9 hours in the PRESTORM and TOGA COARE simulations, and 5 hours in the CRYSTAL-FACE simulation.

Table 5: Summary of precipitation sensitivity (dP) to increases in the number of CCN (dN_0) for different studies. Note that *Van den Heever et al.* [2006] used a linear CCN concentration profile that ranged from $300cm^{-3}$ at 4km above ground level to $1000cm^{-3}$ near the surface; GCCN and IN effects in *Van den Heever et al.* [2006] and *Teller*

and Levin [2006] are excluded from the table; only five of the total 30 cases in *Wang* [2005] are displayed in the table.

Figure Captions

Figure 1: Observed and simulated radar reflectivity for the PRESTORM, TOGA COARE, and CRYSTAL-FACE cases under dirty and clean conditions. **(a)** PRESTORM clean; **(b)** PRESTORM dirty; **(c)** PRESTORM observed (adapted from *Rutledge et al.,* [1988]); **(d)** TOGA COARE clean; **(e)** TOGA COARE dirty; **(f)** TOGA COARE observed (courtesy of Dr. D. Jorgensen from NOAA/NSSL) ; **(g)** CRYSTAL clean; **(h)** CRYSTAL dirty; **(i)** CRYSTAL observed (courtesy of J. Heymsfield from NASA/GSFC).

Figure 2: Time series of GCE model-estimated domain mean surface rainfall rate (mm h^{-1}) for the **(a)** PRESTORM, **(b)** TOGA COARE, and **(c)** CRYSTAL case. The solid/dashed line represents clean/dirty conditions.

Figure 3: Time series of GCE model-simulated maximum vertical velocity (m s^{-1}) for the **(a)** PRESTORM, **(b)** TOGA COARE, and **(c)** CRYSTAL case. The solid/dashed line represents clean/dirty conditions.

Figure 4: Probability distribution function (PDF) of rainfall intensity for the **(a)** PRESTORM, **(b)** TOGA COARE and **(c)** CRYSTAL cases. The grey and black bars represent clean and dirty conditions, respectively.

Figure 5: Same as Fig. 2 except for sensitivity tests without ice processes (warm rain only): **(a)** PRESTORM, **(b)** TOGA COARE, and **(c)** CRYSTAL.

Figure 6: Integrated total water and ice path (kg m^{-2}) averaged every hour for clean (white) and dirty (grey) conditions. The hatched portion of each bar represents the cloud water and pristine ice content. **(a)** PRESTORM water; **(b)** PRESTORM ice; **(c)**

TOGA COARE water; **(d)** TOGA COARE ice; **(e)** CRYSTAL water; **(f)** CRYSTAL ice.

Figure 7: Schematic diagram showing the physical processes that lead to either enhancement (TOGA COARE case) or suppression (PRESTORM case) of precipitation in a dirty environment.

Figure 8: Domain average evaporation rate (day^{-1}) profiles during the two hour of simulation for the **(a)** PRESTORM and **(b)** TOGA COARE case. The solid/dashed line represents the dirty/clean scenario.

Properties	High CCN (Dirty)	Low CCN (Clean)	References (Observations)
Cloud droplet size distribution	Narrower	Broader	*Rosenfeld and Lensky* [1998], *Rosenfeld* [1999 & 2000], *Rosenfeld et al.* [2001], *Rosenfeld and Woodley* [2000], *Andreae et al.* [2004], *Koren et al.* [2006],
Warm-rain process	Suppressed	Enhanced	*Rosenfeld* [1999 & 2000], *Rosenfeld and Woodley* [2000], *Rosenfeld and Ulbrich* [2003], *Andreae et al.* [2004], *Linn et al.* [2006]
Cold-rain process	Enhanced	Suppressed	*Rosenfeld and Woodley* [2000], Orville et al. [2001], Williams *et al.* [2002], *Andreae et al.* [2004], *Linn et al.* [2006], *Bell et al.* [2007]
Mixed phase region	Deeper	Shallower	*Rosenfeld and Lensky* [1998], Williams *et al.* [2002], *Linn et al.* [2006]
Cloud-top height	Higher	Lower	*Andreae et al.* [2004], *Koren et al.* [2006], *Linn et al.* [2006]
Lightning	Enhanced (downwind side)/higher max flash	Less and lower max flash	*Williams et al.* [2002], *Orville et al.* [2001]

Table 1 Key observational studies identifying the differences in the microphysical properties, cloud characteristics, thermodynamics, and dynamics associated with clouds and cloud systems developed in dirty and clean environments.

		Microphysics	Turbulence	Radiation	Domain	Grid Size & Time step	Lateral Boundary Conditions	Cases	Integration
Khain et al. [2004]	2-D	Spectral Bin (33 bin) 6 types of ice	1st order	No	64 x 16 km	dx=250 m dz=125 m dt=5 s	Closed	A squall lines (E. Atlantic) and a convective cloud (Texas)	~2 h
Khain and Pokrovsky [2004]	2-D	Spectral Bin (33 bin) 6 types of ice	1st order	No	64 x 16 km	dx=250 m dz=125 m dt=5 s	Closed	A convective cloud (Texas)	2.5 h
Khain et al. [2005]	2-D	Spectral Bin (33 bin) 6 types of ice	1st order	No	128 x 16 km	dx=250 m dz=125 m dt=5 s	Closed	Two squall lines (E. Atlantic and Oklahoma) and a convective cloud (Texas)	2 and 4 h
Fridlind et al. [2003]	3-D	Spectral Bin (16 bins) 1 type of ice	1st order	No	48 x 48x 24 km	dx=dy=500 m dz=375 m dt=5 s	Closed	A convective cloud (Florida)	3 h
Wang [2005]	3-D	Two moment bulk scheme	1st order	6 Broad Bands for Solar and 12 for IR. Four-stream discrete-ordinate scattering, k-distribution	400 x 200x 25 km	dx=dy=2000 m dz=500 m dt=5 s	Cyclic	A squall line (ITCZ)	4 h
Van den Heever et al. [2006]	3-D	Two moment bulk scheme	1st order	A broad-band two-stream for solar and an emissivity for IR	145 x 145x 20km	dx=dy=500 m dz= stretched dt=1 s	Radiative Open	Thunderstorm (CRYSTAL-FACE)	12h
Cheng et al. [2006]	3-D	Two moment bulk scheme (Warm rain only)	1st order	A simple broad-band solar and emissivity (IR)	810 x 810 km x 100 Pa	dx=dy= 3000m dz=stretched dt=5 s	Radiative Open	A shallow Stratus (ARM-SGP)	72 h
Lynn et al. [2005]	3-D	Spectral Bin (33 bin) 3 types of ice and Bulk scheme	TKE	A broad-band two-stream for solar and an emissivity for IR	400 x 199 x 25 km	dx=dy=1000 m dz=stretched dt=9 s	Radiative Open	A squall line (Florida)	13 h
Fan et al. [2006]	2-D	Spectral Bin (33 bin) 6 types of ice	TKE	No	512 x 22 km	dx=500 m dz=stretched (250 – 1260 m) dt=6 s	Radiative Open	A sea-breeze induced convective event (Houston, Tx)	3 h
Teller and Levin [2006]	2-D	Spectral Bin (33 bin) 3 types of ice	1st order	No	30 x 8 km	dx=300 m dz=300 m dt=2 s	Closed	Winter convective cloud Eastern Mediterranean	80 minutes
Van den Heever and Cotton [2007]	3-D	Two moment bulk scheme	1st order	A broad-band two-stream for solar and an emissivity for IR	228 x 228x 22km	dx=dy=1500 m dz= stretched dt=2 s	Radiative Open	Thunderstorm (St. Louis)	26h

Table 2 Key papers using CRMs to study the impact of aerosols on precipitation. Model dimensionality (2D or 3D), microphysical schemes (spectral-bin or two-moment bulk), turbulence parameterization (1st or one and a half order TKE), radiation (with or without), domain size (km), resolution (m), time step (seconds), lateral boundary condition (closed, cyclic or radiative open), case and integration time (hours) are all listed.

	Location	System Type	CAPE m^2s^{-2}	Precipitable Water ($g\ cm^{-2}$)	References
TOGA COARE (February 22 1993)	Tropical Pacific	MCS	1776	6.334	Wang *et al.* 1996, 2003; Tao *et al.* 2003; Lang *et al.* 2003
PRESTORM (June 10-11 1985)	Oklahoma	MCS	2300	4.282	Tao *et al.* 1995, 1996; Lang *et al.* 2003
CRYSTAL-FACE (July 16 2002)	Florida	Sea Breeze Convection	2027	4.753	This paper

Table 3 Initial environmental conditions expressed in terms of CAPE (convective available potential energy) and precipitable water for the TOGA COARE, PRESTORM and CRYSTAL-FACE case. The geographic locations, storm type and previous modeling papers are also shown.

	TOGA COARE Clean (100)	TOGA COARE Dirty (2500)	PRESTORM Clean (600)	PRESTORM Dirty (2500)	CRYSTAL Clean (600)	CRYSTAL Dirty (2500)
Averaged Rain (mm/day/grid)	18.0	28.4	38.3	29.1	12.6	11.0
Stratiform (%)	50	17	43	70	43	40
Precipitation Efficiency - PE (%)	65	52	33	26	33	28
Ice water path ratio	.52	.65	.86	.88	.75	.79

Table 4 Domain-averaged surface rainfall amount (in mm day^{-1}), stratiform percentage (in %), precipitation efficiency (PE in %), and ice water path ratio (ice water path divided by the total liquid and ice water path) for the TOGA COARE, PRESTORM and CRYSTAL-FACE case under dirty and clean conditions. Note there are 9 hours in the PRESTORM and TOGA COARE simulations, and 5 hours in the CRYSTAL-FACE simulation.

Reference	case	dN_0 (N_{clean}) [cm^{-3}]	dP (%)
This study	TOGA COARE	2400 (100)	+58.
	PRESTORM	1900 (600)	-24.
	CRYSTAL	1900 (600)	-13.
***Phillips et al.* [2002]**	New Mexico	1950 (800)	-14.
		4200 (800)	-30.
***Khain et al.* [2004]**	GATE	1160 (100)	-3.
***Khain and Pokrovsky* [2004]**	Texas	40 (10)	-16.
		90 (10)	-19.
		290 (10)	-53.
		1250 (10)	-88.
***Khain et al.* [2005]**	PRESTORM	1160 (100)	+258.
***Teller and Levin* [2006]**	Winter-time eastern Mediterranean	210 (100)	-27.
		510 (100)	-55.
		810 (100)	-73.
		1260 (100)	-93.
***Wang* [2005]**	ITCZ	400(100)	+180.
		800 (100)	+340.
		1200(100)	+540.
		1500 (100)	+700.
***Lynn et al.* [2005]**	Florida	1250 (10)	-5.
***Van den Heever et al.* [2006]**	CRYSTAL	350 (300)	-22.

Table 5 Summary of precipitation sensitivity (dP) to increases in the number of CCN (dN_0) for different studies. Note that *Van den Heever et al.* [2006] used a linear CCN concentration profile that ranged from 300cm^{-3} at 4km above ground level to 1000cm^{-3} near the surface; GCCN and IN effects in *Van den Heever et al.* [2006] and *Teller and Levin* [2006] are excluded from the table; only five of the total 30 cases in *Wang* [2005] are displayed in the table.

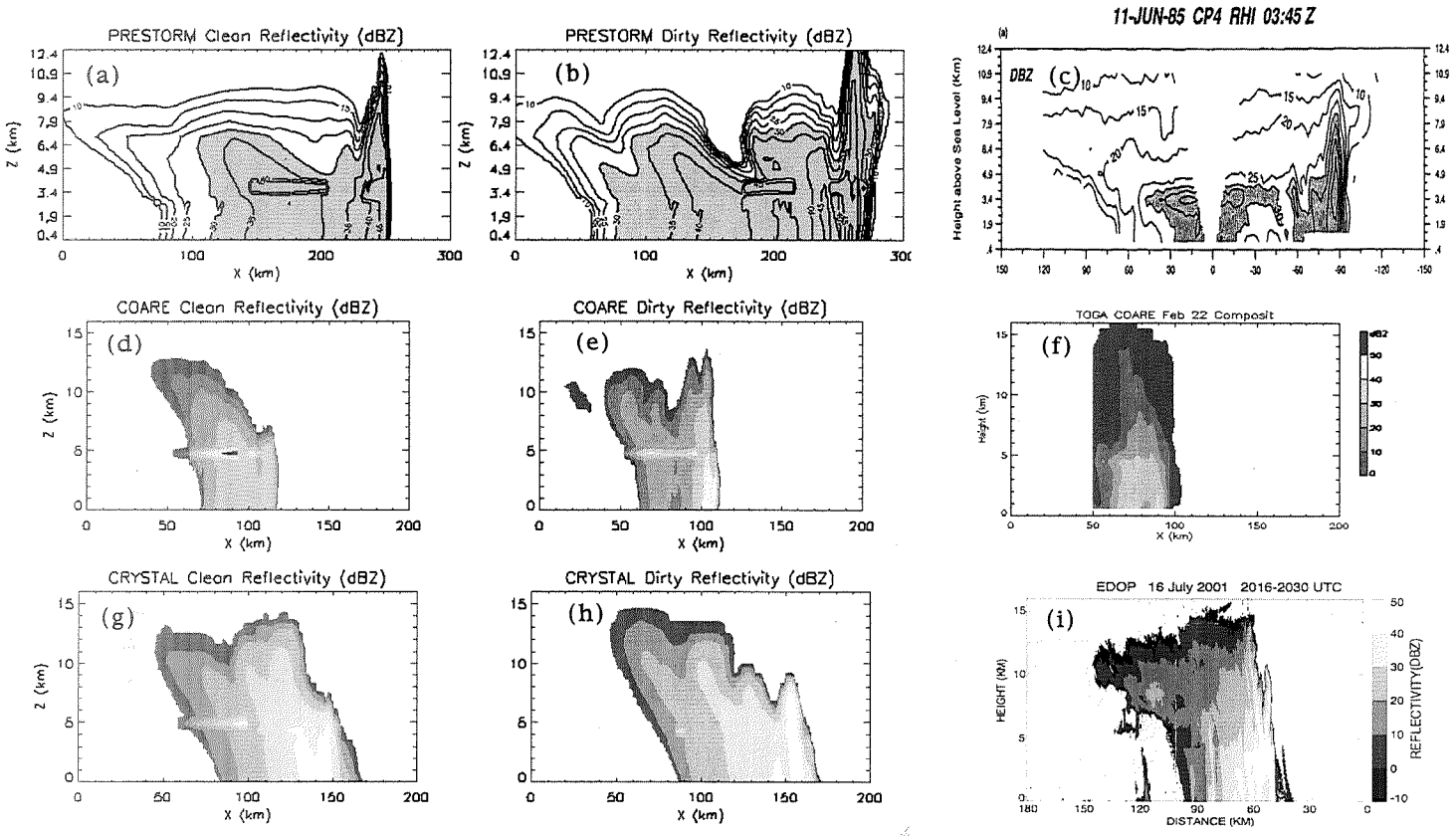

Fig. 1 Observed and simulated radar reflectivity for the PRESTORM, TOGA COARE, and CRYSTAL-FACE cases under dirty and clean conditions. **(a)** PRESTORM clean; **(b)** PRESTORM dirty; **(c)** PRESTORM observed (adapted from *Rutledge et al.,* [1988]); **(d)** TOGA COARE clean; **(e)** TOGA COARE dirty; **(f)** TOGA COARE observed (courtesy of D. Jorgensen from NOAA/NSSL) ; **(g)** CRYSTAL clean; **(h)** CRYSTAL dirty; **(i)** CRYSTAL observed (courtesy of J. Heymsfield from NASA/GSFC).

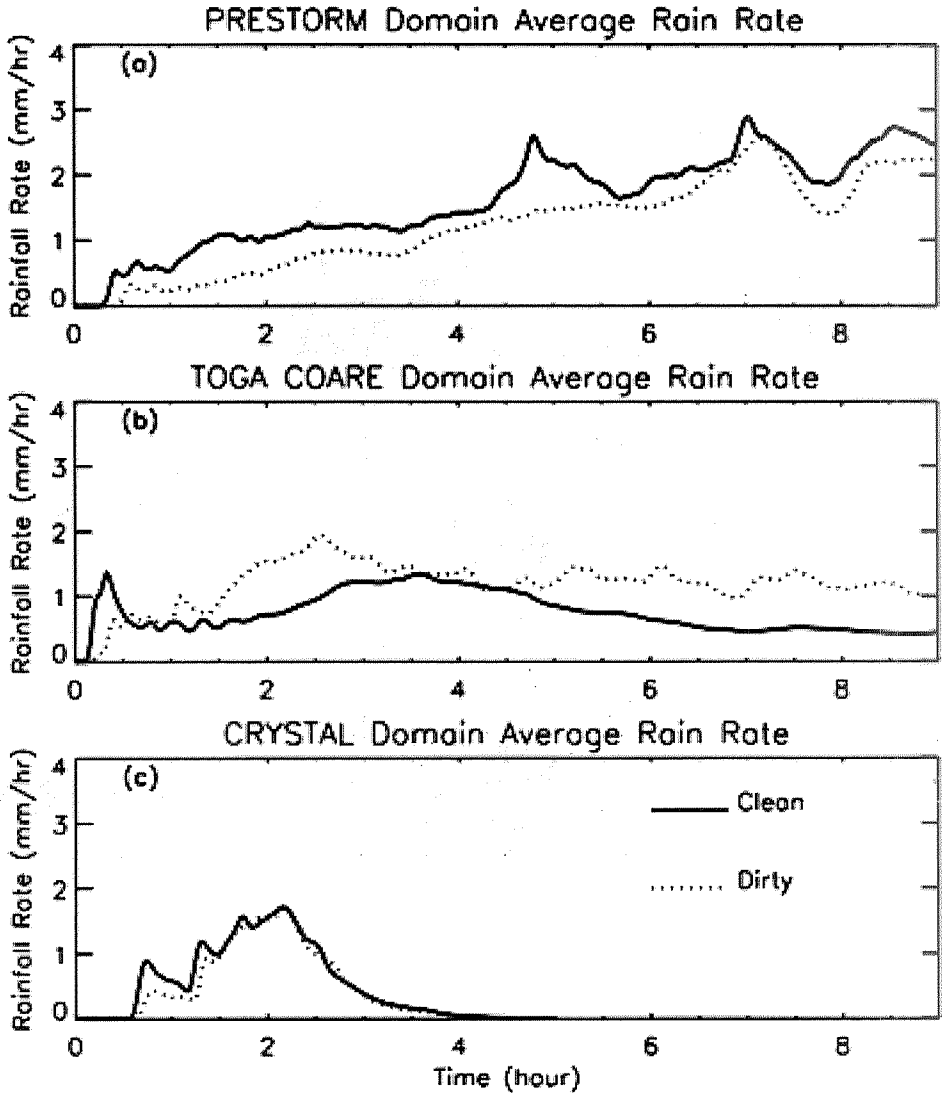

Fig. 2 Time series of GCE model-estimated domain mean surface rainfall rate (mm h^{-1}) for the **(a)** PRESTORM, **(b)** TOGA COARE, and **(c)** CRYSTAL case. The solid/dashed line represents clean/dirty conditions.

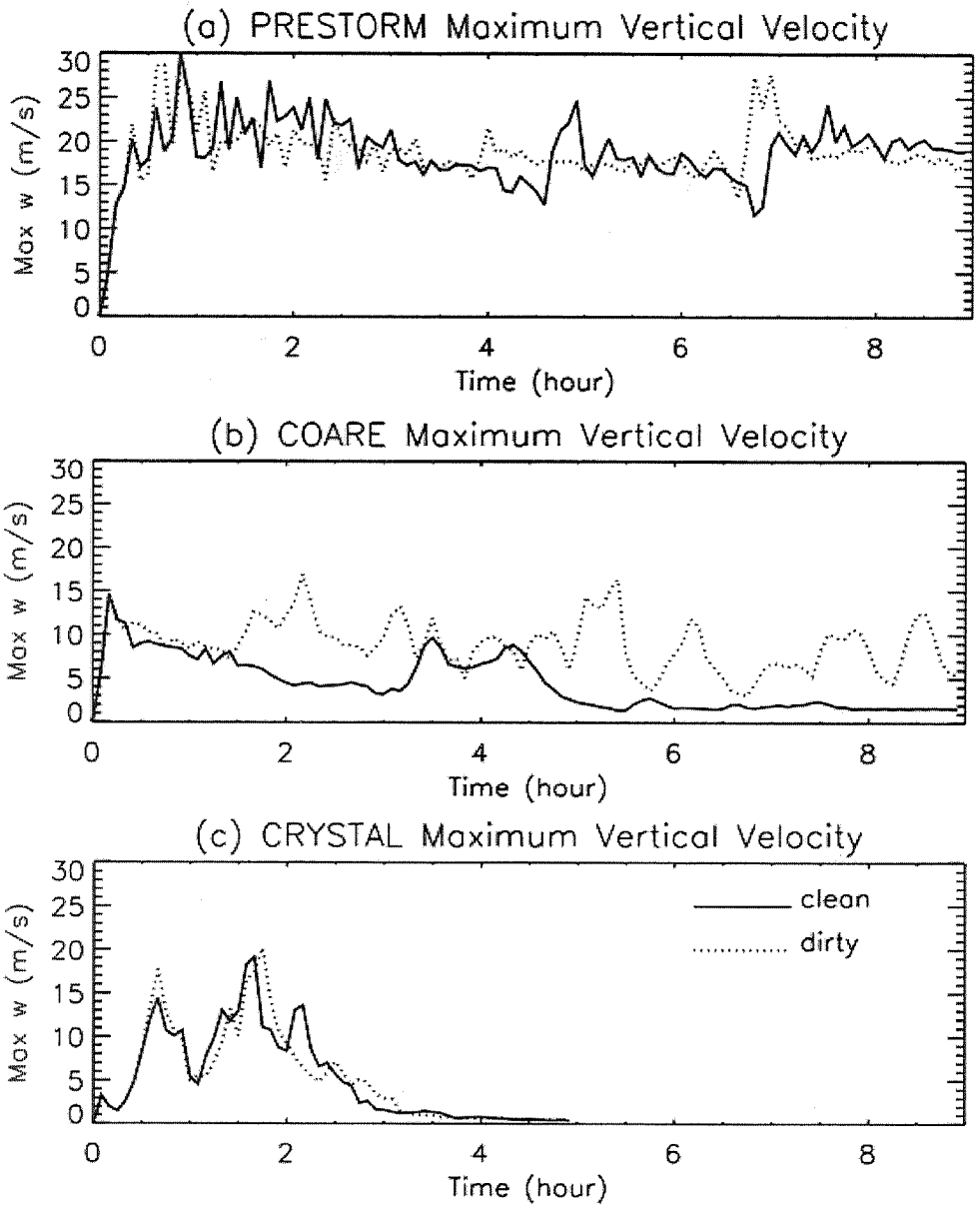

Fig. 3 Time series of GCE model-simulated maximum vertical velocity (m s^{-1}) for the (a) PRESTORM, (b) TOGA COARE, and (c) CRYSTAL case. The solid/dashed line represents clean/dirty conditions.

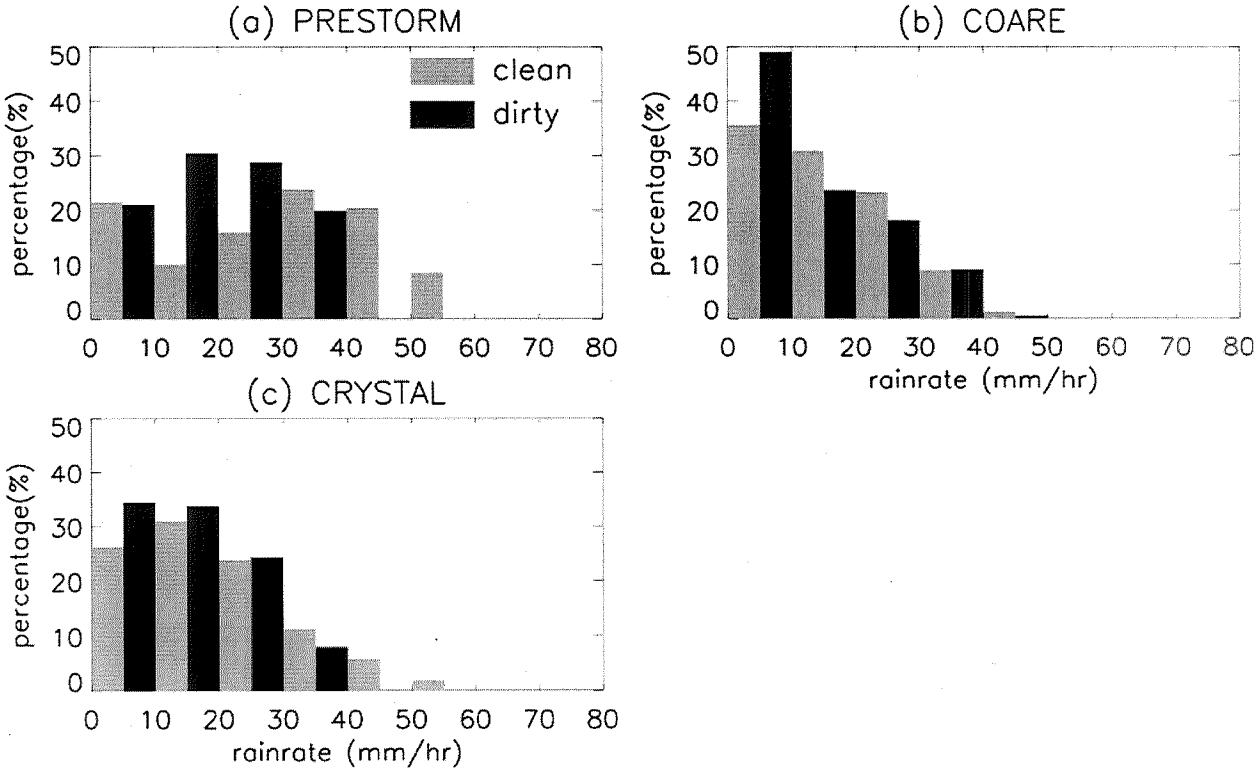

Fig. 4 Probability distribution function (PDF) of rainfall intensity for the **(a)** PRESTORM, **(b)** TOGA COARE and **(c)** CRYSTAL cases. The grey and black bars represent clean and dirty conditions, respectively.

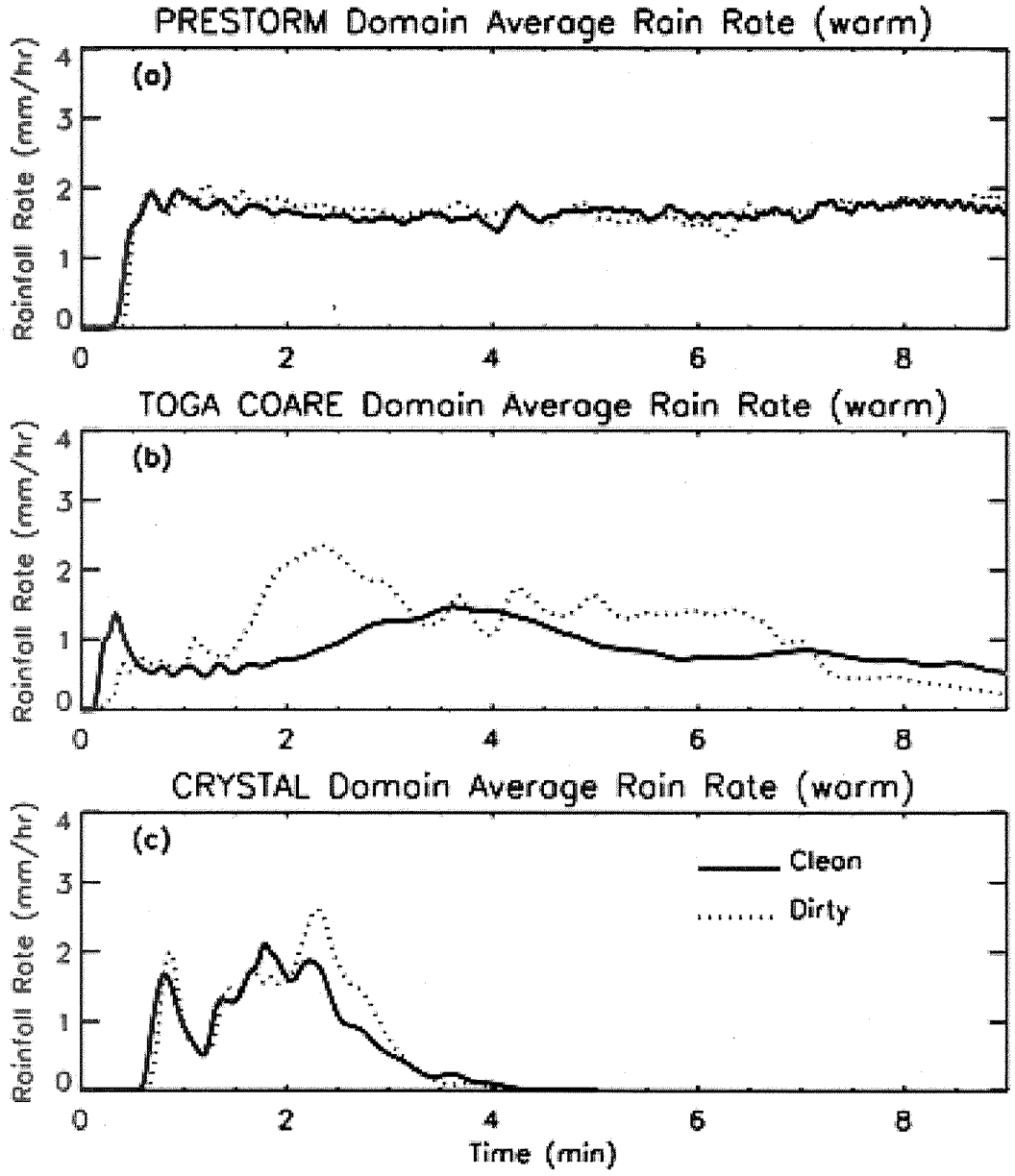

Fig. 5 Same as Fig. 2 except for sensitivity tests without ice processes (warm rain only): **(a)** PRESTORM, **(b)** TOGA COARE, and **(c)** CRYSTAL.

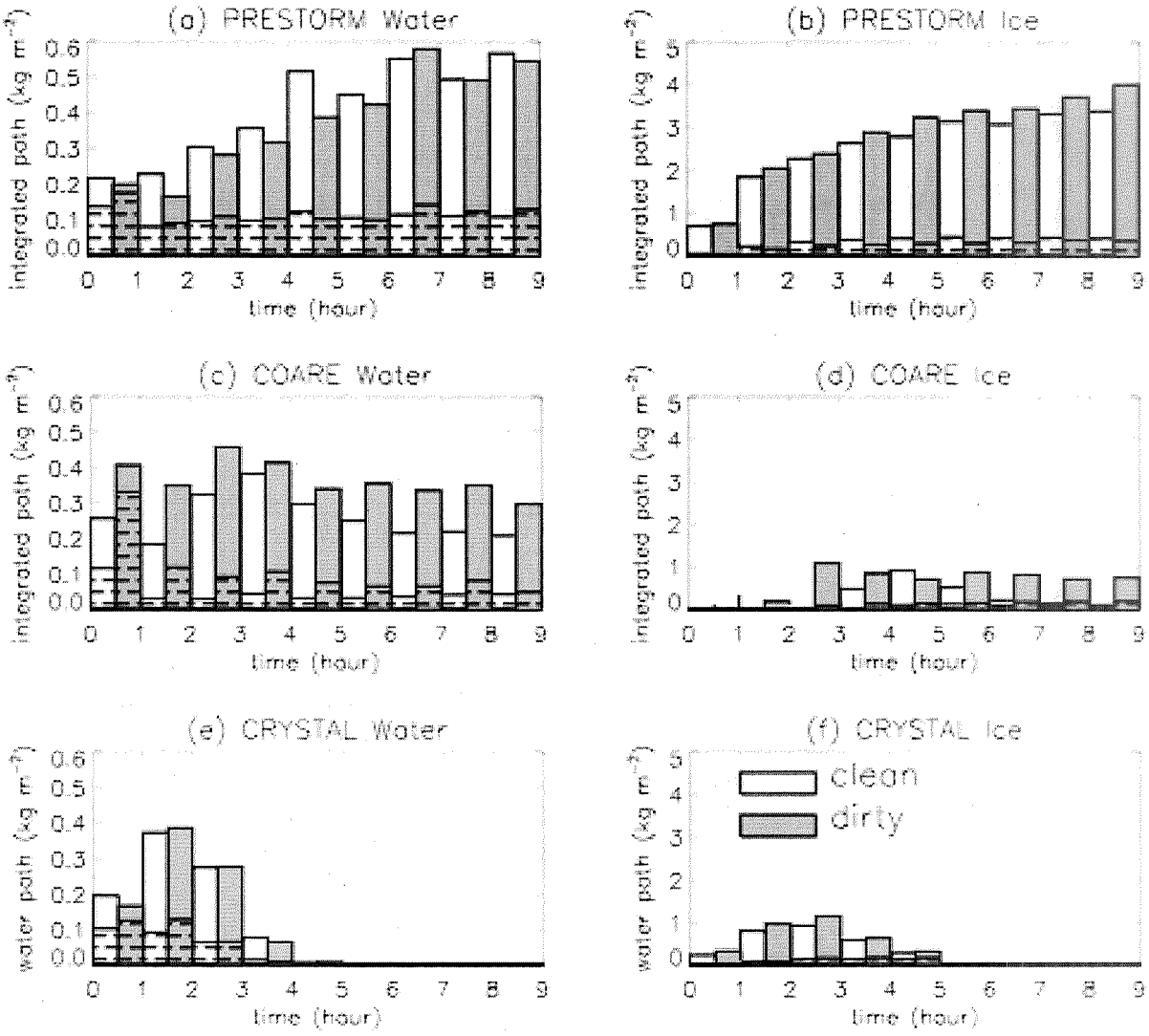

Fig. 6 Integrated total water and ice path (kg m^{-2}) averaged every hour for clean (white) and dirty (grey) conditions. The hatched portion of each bar represents the cloud water and pristine ice content. **(a)** PRESTORM water; **(b)** PRESTORM ice; **(c)** TOGA COARE water; **(d)** TOGA COARE ice; **(e)** CRYSTAL water; **(f)** CRYSTAL ice.

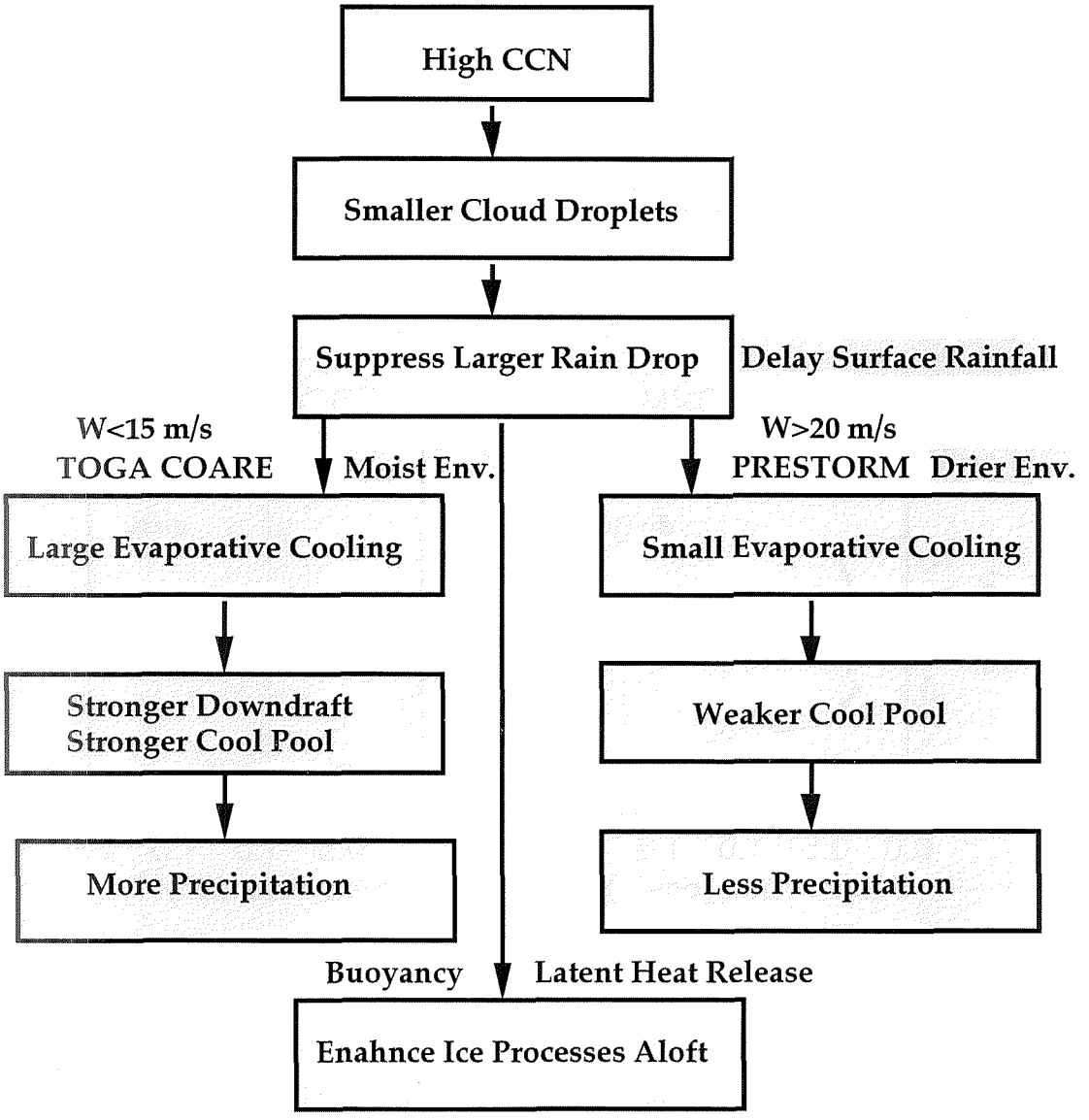

Fig. 7 Schematic diagram showing the physical processes that lead to either enhancement (TOGA COARE case) or suppression (PRESTORM case) of precipitation in a dirty environment.

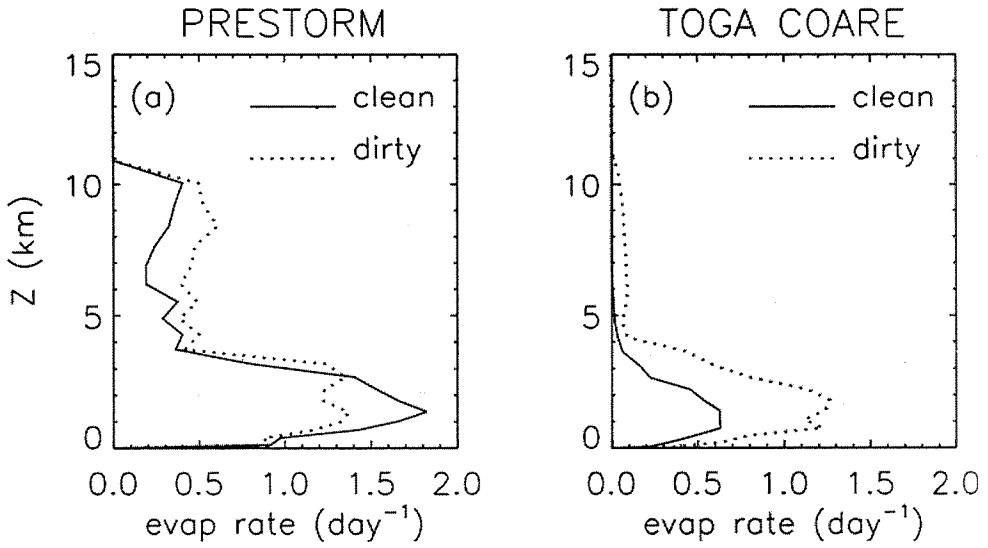

Fig. 8 Domain average evaporation rate (day^{-1}) profiles during the first two hour of simulation for the **(a)** PRESTORM and **(b)** TOGA COARE case. The solid/dashed line represents the dirty/clean scenario.